Study on stretching liquid bridges with symmetric and asymmetric surface wettability

Jiayi Zhao [1] Nan Zhou,[2] Kaixuan Zhang,[2] Shuo Chen [2,*] and Yang Liu [3]

[1]*School of Energy and Power Engineering, University of Shanghai for Science and Technology, Shanghai 200093, China*
[2]*School of Aerospace Engineering and Applied Mechanics, Tongji University, Shanghai 200092, China*
[3]*Department of Mechanical Engineering, The Hong Kong Polytechnic University, Hung Hom, Hong Kong, China*

The breakup process of stretching liquid bridges between plates is crucial for liquid transfer in printing technology. In the present study, the liquid bridges stretched by two parallel flat plates were simulated by using many-body dissipative particle dynamics, in which the competition between slip velocity of contact lines and thinning velocity of liquid bridges was focused on, and it shows that this competition plays a key role in determining the breakup behaviors of liquid bridges and the liquid transfer ratio between the two plates. The influences of surface wettability, plate stretching velocity, and liquid Oh number on the breakup process were discussed. The simulated results show that both poorer surface wettability and larger stretching velocity help to increase slip velocity and enable the liquid bridge to slip off the surfaces. For the case with hydrophilic surface and small plate stretching velocity, thinning velocity dominates the breakup process and the pinch-off occurs approximately at the middle part of the liquid bridge. For cases with asymmetric surface wettability, the liquid transfer ratio depends only on the asymmetry of surface wettability for smaller plate stretching velocity and larger Oh number. However, this phenomenon no longer occurs if the stretching velocity is increasing, where slip of the contact line becomes important. The shift of minimal radius for liquid bridges with asymmetric stretching velocities is also investigated, and it was found that the shift moment is only related to the surface wettability, regardless of the plate stretching velocity. Moreover, it shows that the formation of satellite drops depends on the sequential order of the appearance of the liquid bridge slipping off the surface and the breakup of the filament. The present work provides some insight to better understand the rupture mechanism of stretching liquid bridges, and may help to improve printing technology.

I. INTRODUCTION

The pioneering work for rupture of liquid bridges may date back to the second half of the nineteenth century, carried out by Plateau [1], Rayleigh [2,3], and others. Their stability analysis showed that the perturbations imposed on an indefinitely long liquid bridge would become linearly unstable if the wavelength exceeds the circumference of the jet, and the liquid column would then spontaneously decay into drops. This behavior is crucial in practical applications, especially in the area of inkjet printing [4,5], where the printing efficiency relies on liquid transfer from the printing plate surface to the targeted substrate. High quality liquid transfer requires the liquid bridge to slip

*schen_tju@tongji.edu.cn

completely off the surface, so the dynamics of moving contact lines is crucial in the liquid stretching process.

Kröger *et al.* [6] experimentally studied the stretching behaviors of larger polymeric and Newtonian liquid bridges, showing that the breakup of liquid bridges is slowed down under the condition of high elongational viscosity and the rupture behaviors vary with the liquid properties. Zhang *et al.* [7] analyzed the nonlinear dynamics of an axisymmetric stretching liquid bridge. They found that the limiting length, i.e., the maximum distance between the plates as the liquid bridges reach breakup, increases significantly with large liquid viscosity and stretching velocity. Furthermore, a kind of two-step mechanism for liquid transfer in the stretching process was proposed by Gupta *et al.* and a qualitative model describing the physics of the liquid transfer between hydrophobic surfaces was proposed [8]. Dodds *et al.* provided a two-dimensional (2D) Galerkin–finite element method to study the influences of surface wettability on liquid transfer ratio [9], and they also investigated the role of inertia in stretching liquid bridges with moving contact lines [10]. In particular, Qian and Breuer [11] carried out experimental and numerical studies on dynamics of contact lines of a stretching liquid bridge. They pointed out that the competition between the slip velocity of the contact line and the thinning velocity of the liquid bridge plays a key role in liquid transfer, and it is necessary to further systematically investigate the influences of various factors.

Additionally, when jet diameters reach molecular size, the rupture behavior of liquid bridges is believed to be dominated by thermal fluctuations [12–15], where conventional linear stability theory is of questionable validity. As the experimental measurements are subject to temporal and spatial resolution, the thermal length of liquids is hard to observe at laboratory scale [16,17]. Moseler and Landman proposed a stochastic modification for the deterministic lubrication equation (SLE) in order to describe the effects of thermal fluctuations [18], where the double-cone neck shapes before pinching off could be captured, while it is absent in LE. Moreover, the results provided by molecular dynamics (MD) were proved to be consistent with the predictions of SLE [19]. However, relatively high computational cost is an obstacle to the feasibility of MD to deal with problems in multiple scales [20,21].

On the other hand, the Gaussian noise in SLE obeys the fluctuation dissipation theorem (FTD) [22], and this theorem could also be depicted by the mesoscopic particle-based method, dissipative particle dynamics (DPD) [23–26]. Hence, DPD is believed to be able to capture the crossover between hydrodynamics and thermal fluctuation domination [27]. Actually, Tiwari and Abraham [28] first utilized modified DPD by introducing an additive surface tension term into the conservative force to explore the clogging of nanojets near nozzles. Their outcome is in agreement with the results of MD, indicating that thermal fluctuation phenomena at the submicron level can be described successfully in DPD. They also continued to summarize the relation between the breakup time of the liquid nanocylinders and the thermal length scale [21].

In the present study, a derivative method from DPD, named many-body dissipative particle dynamics (MDPD) [29,30], was adopted. MDPD can generate the coexistence of vapor and liquid with a sharp interface when compared with the modified DPD method proposed by Tiwari *et al.* MDPD has been validated to be able to describe the liquid bridge dynamics from potential and inertial-viscous, to stochastic flow [31]. Accordingly, various studies on droplet dynamics with moving contact lines by MDPD were carried out [32–35]; for example, it shows that the dynamic contact angle and capillarity driven imbibition simulated by MDPD are consistent both with theories of Cox and the Lucas-Washburn equation [36–38], and MDPD could be considered as a feasible tool for investigating the stretching process of liquid bridges.

The present study aims to quantitatively analyze the competition between the slip of the contact line and the thinning behavior of stretching liquid bridges, in which the surface wettability, plate stretching velocity, and the liquid Oh number are taken into consideration, and the liquid transfer ratio between two plates is also investigated, which is the core of most printing processes.

The article is organized as follows. In Sec. II we briefly introduce the simulation method and verify the model by comparing the simulated profile of the liquid bridge and its spontaneous rupture
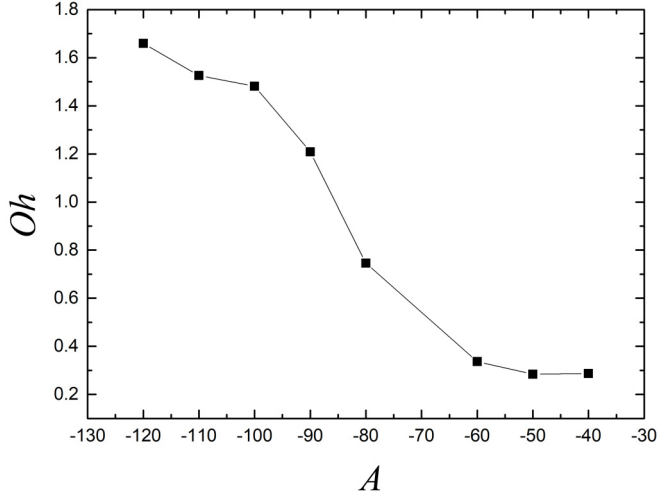
FIG. 1. The relation between attractive coefficient A and Oh number with repulsive coefficient B fixed at 25.

process with theoretical predictions. In Sec. III, the stretching process between two plates with symmetric surface wettability is discussed and the competition between the slip of the contact line and the thinning behavior of the liquid bridge is analyzed. Then, the influences of asymmetric surface wettability and plate stretching velocity on the rupture dynamics of a liquid bridge and liquid transfer ratio are presented. Finally, we give a brief conclusion in Sec. IV.

II. MODEL AND VALIDATION

A. Simulation method

As a derivative method from DPD, many-body dissipative particle dynamics (MDPD) introduces the van der Waals loop into the equation of state (EOS) to make it suitable for simulating the free liquid-vapor interface. MDPD modifies the form of traditional conservative force as

$$\boldsymbol{F}_{ij}^{C} = [Aw_C(r_{ij}) + B(\bar{\rho}_i + \bar{\rho}_j)w_d(r_{ij})]\boldsymbol{e}_{ij}, \tag{1}$$
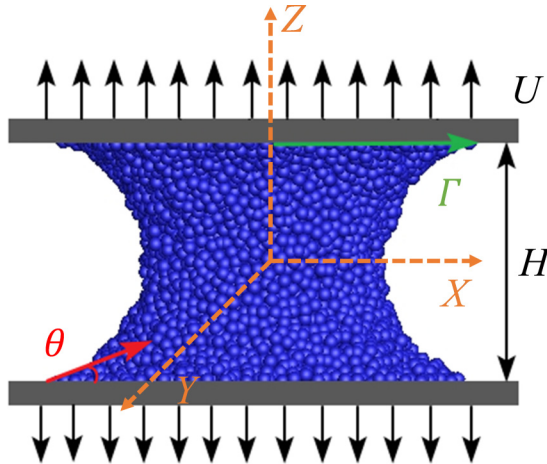

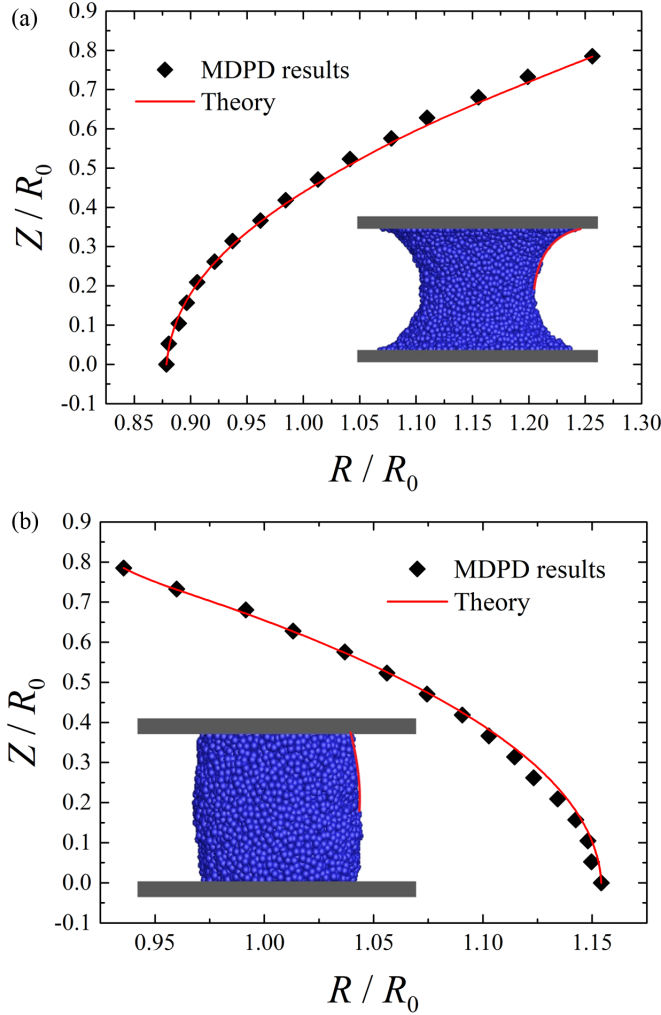FIG. 2. Schematic diagram of a stretching liquid bridge between two flat plates.

FIG. 3. The comparison of liquid bridge profiles between theoretical predictions and simulation results. (a) hydrophilic surface with $\theta = 30°$. (b) Hydrophobic surface with $\theta = 100°$.

where the local density of particle i, i.e., $\bar{\rho}_i$, is added into the conservative force. The value of the local density is calculated by the weight function $w_\rho(r_{ij}) = \frac{15}{2\pi r_d^3}(1 - \frac{r_{ij}}{r_d})^2$, which depends on the distance r_{ij} between particle pairs. The strengths of the attractive and repulsive force are controlled by corresponding coefficients A and B. $w_C(r_{ij})$ and $w_d(r_{ij})$ are the weight functions depending on the distance r_{ij} and will decrease to zero when $r_{ij} \geqslant r_c$ for $w_C(r_{ij})$ and $r_{ij} \geqslant r_d$ for $w_d(r_{ij})$. The dissipative and random forces are the same with traditional DPD.

The properties of MDPD liquids are influenced by the choice of parameters in Eq. (1). For simplicity, the repulsive coefficient B is fixed at 25 as in previous MDPD simulations. Then the attractive coefficient A is changed to generate different values of surface tension σ, viscosity μ, and density ρ of liquids. The surface tension is calculated by the fitting equation provided by Arienti [31] as

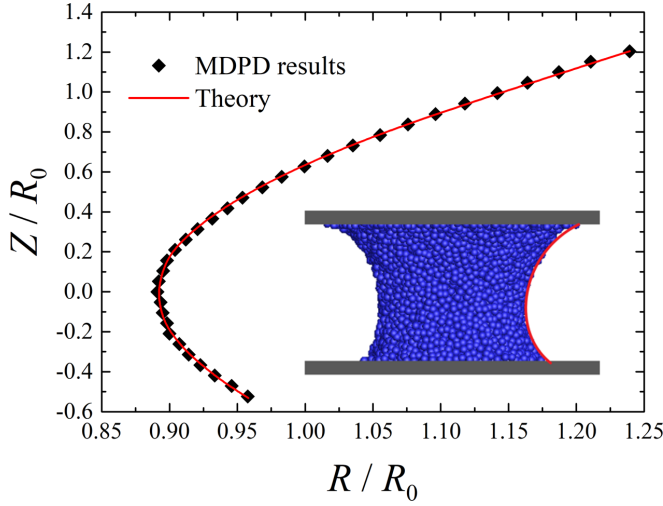$$\sigma^{\text{fit}} = -\frac{\pi}{240}\left(0.42 A r_c^5 \rho^2 + 0.0030 B r_d^5 \rho^3\right), \tag{2}$$

FIG. 4. The comparison of liquid bridge profiles with asymmetric wettability, where $\theta_{\text{upper}} = 30°$ and $\theta_{\text{lower}} = 55°$.

and the viscosity is obtained from the shear flow simulation with the Lees-Edwards boundary condition, as described in our previous work in detail [35]. The Ohnesorge number (Oh) is adopted to express the relation between surface tension and viscosity of liquids. Oh is defined as

$$\text{Oh} = \frac{\mu}{\sqrt{\rho \sigma R_0}}, \tag{3}$$

where R_0 is the characteristic length. In the present simulation, R_0 is the radius of the free liquid cylinder as follows:
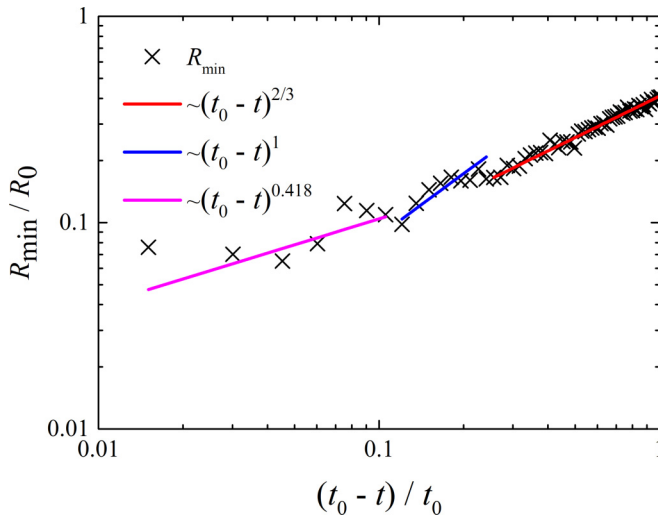
$$R_0 = \sqrt{\frac{N}{\pi \rho H_0}}, \tag{4}$$

FIG. 5. Variation of the minimum radius of the thread versus time with the power law of the three flows, i.e., potential flow (2/3), inertial-viscous flow (1.0), and stochastic flow (0.418).
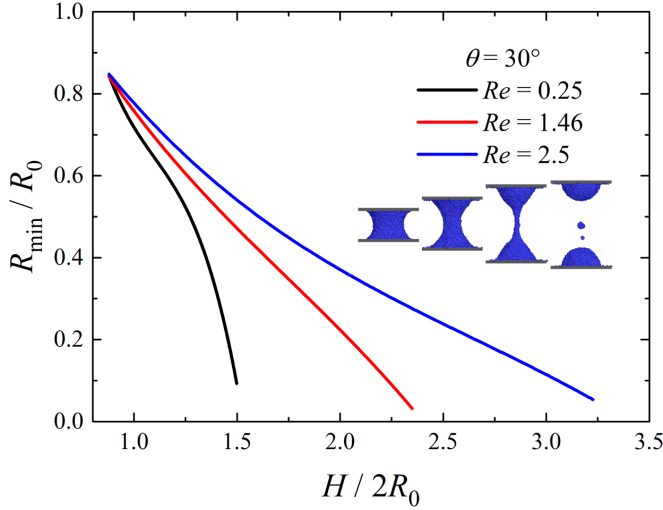
FIG. 6. Minimum radius versus the distance between the plates with different Re.

where N is the particle number and H_0 is the initial height between two plates. We achieve the relation between A and Oh as shown in Fig. 1. Two kinds of liquid, for which Oh = 0.3 and Oh = 0.9, respectively, are selected to analyze the influence of Oh on the process of stretching liquid bridges.

B. Simulation model

Two flat plates are located at both ends of the liquid bridge with different wettability controlled by the solid-liquid attractive coefficient. Six kinds of surfaces are considered, in which the apparent contact angles θ of liquid bridges are 30°, 55°, 70°, 80°, 90°, and 100°, respectively. Invariant plate stretching velocity U is adopted to stretch the liquid bridge along the Z direction. H represents the distance between the two plates, i.e., the liquid bridge length; Γ is the radius of moving contact lines. The schematic diagram of the stretching liquid bridge is shown in Fig. 2.
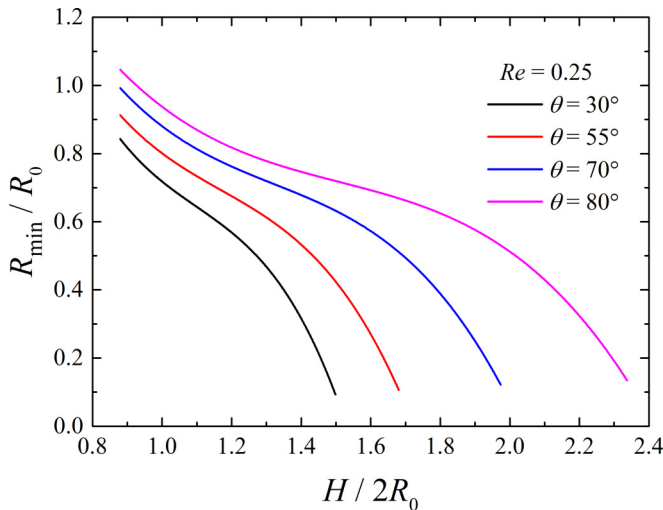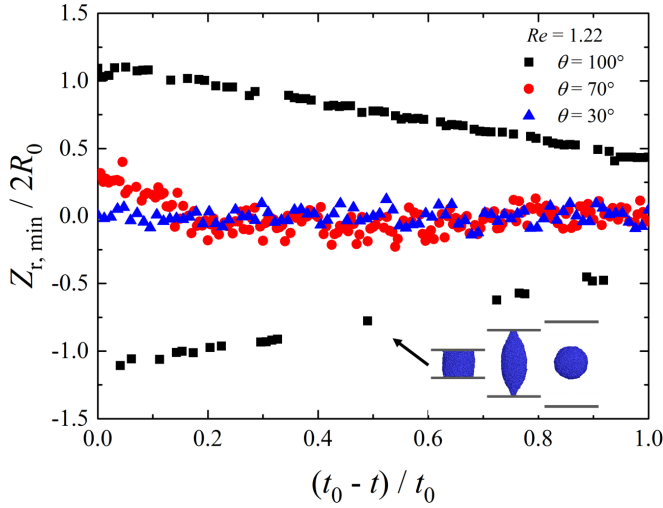

FIG. 7. Variation of minimum radius with H for different surface wettability.

FIG. 8. $Z_{r,min}$ versus breakup time with different θ and Re = 1.22.

C. Validations

The liquid bridge profile is a surface with constant mean curvature if the gravity effect is not considered. Delaunay first proposed an analytical solution of the liquid bridge profile [39]. De Souza *et al.* extended Delaunay's work to analyze the profile of liquid bridges between two chemically different parallel surfaces [40]. The equilibrium profile of the liquid bridge was then computed by Kusumaatmaja *et al.* [41], which is a function of contact angle, liquid volume, and radius of contact area. Recently, Wang *et al.* [42] proposed a profile solution for liquid bridges between parallel surfaces. The profiles of symmetric and asymmetric liquid bridges are calculated according to a constant Laplace pressure and it was experimentally verified by water, Kaydol, and dodecane drops, respectively; the radial coordinate x of the profile is

$$x = \frac{\sin \varepsilon \, \pm \, \sqrt{\sin^2 \varepsilon - 4ac}}{2a}, \tag{5}$$
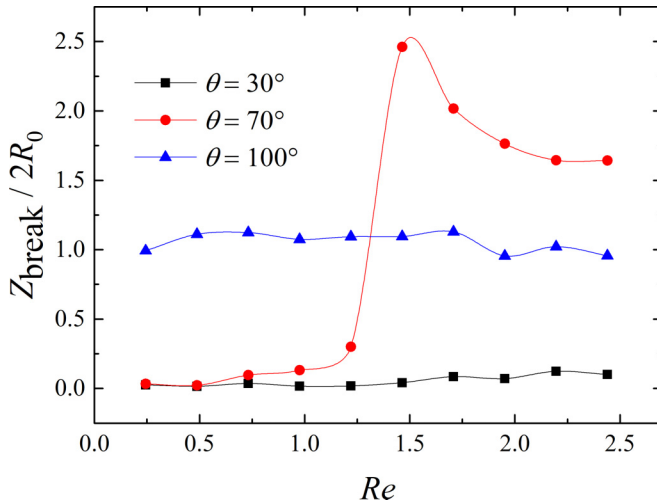
FIG. 9. The variation of the position of the rupture point with Re for different plate wettabilities.
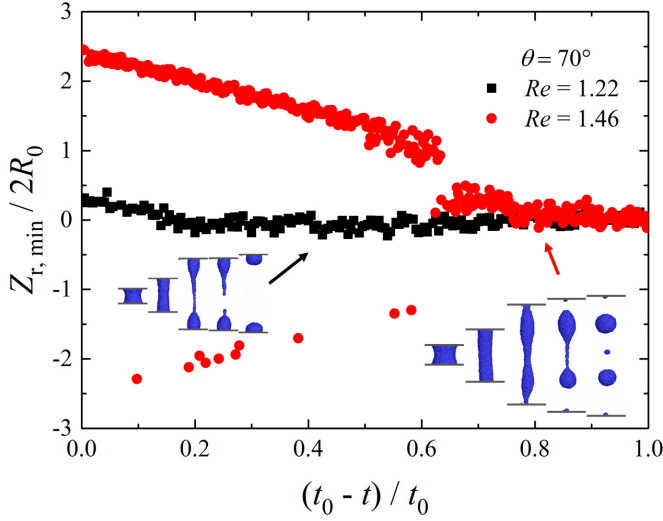
FIG. 10. The variation of $Z_{r,min}$ with time for Re = 1.22 and 1.46.

where $\varepsilon = \pi - \varphi$; φ is the advancing or receding contact angle between the liquid bridge and the surface. The plus sign is for a convex bridge and the minus sign is for a concave bridge. a and c are determined by the boundary condition as follows:

$$a = \frac{x_1 - x_2 \sin \varphi}{x_1^2 + x_2^2}, \tag{6}$$

$$c = x_1 - ax_1^2, \tag{7}$$

where x_1 and x_2 are the radial coordinates at the position of the minimum radius of the profile and the three-phase point, respectively. Then the axial coordinate z is given by the elliptical integrals of
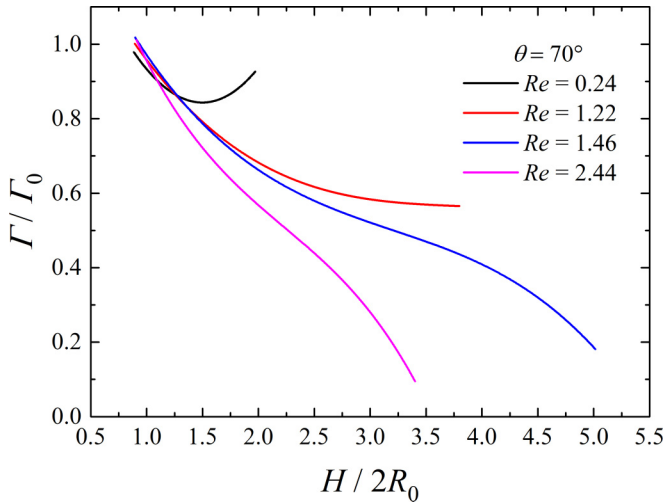
FIG. 11. The radius Γ of the contact line varying with the liquid bridge length.
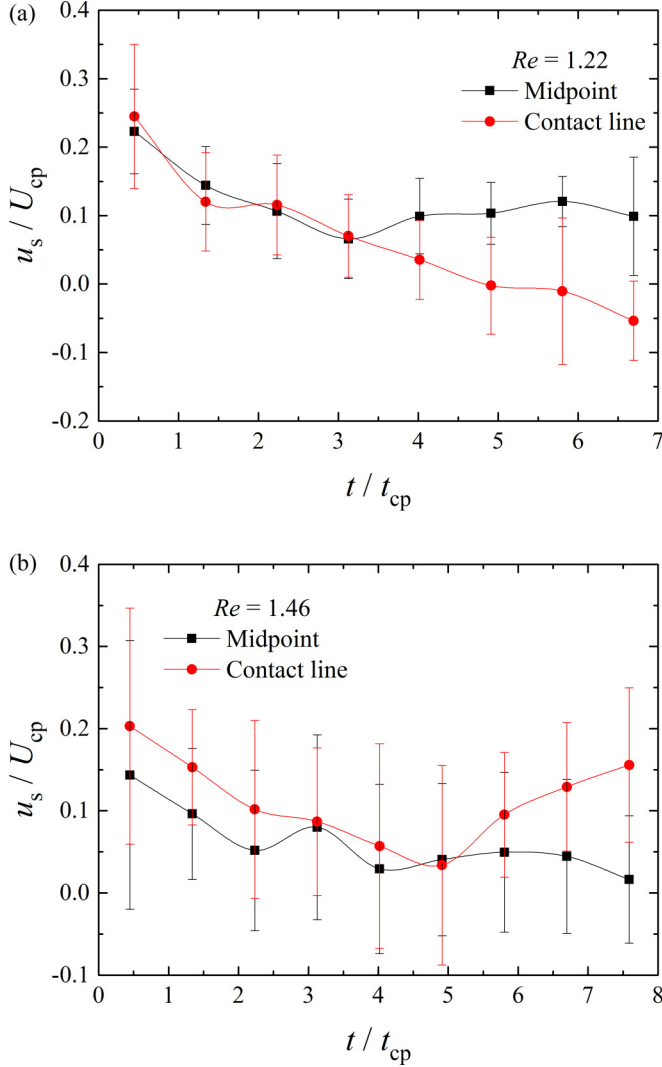
FIG. 12. The evolution of the slip velocity of the contact line and the thinning velocity of the midpoint with Re = 1.22 and 1.46.

the first and second kinds as

$$z = \frac{1}{2a} \int_{\pi/2}^{\varepsilon} \sin \xi \left[-1 \pm \frac{\sin \xi}{\sqrt{\sin^2 \xi - 4ac}} \right] d\xi. \tag{8}$$

Now, the profile of the liquid bridge can be described by the locus of points (x, z) as long as the values of x_1, x_2, and φ are determined. We compare the stable liquid bridge profile obtained from the MDPD simulations with the analytical solutions according to Eqs. (5)–(8). Figure 3 demonstrates that the numerical results are in good agreement with the theoretical predictions for both hydrophilic and hydrophobic surfaces. Moreover, the profile of the liquid bridge between parallel plates with asymmetric wettability is also verified, as shown in Fig. 4.

Spontaneous pinch-off of a liquid cylinder is then simulated by MDPD. The number of particles in the present study is over 13 500, which is believed to obtain the converged results for simulating
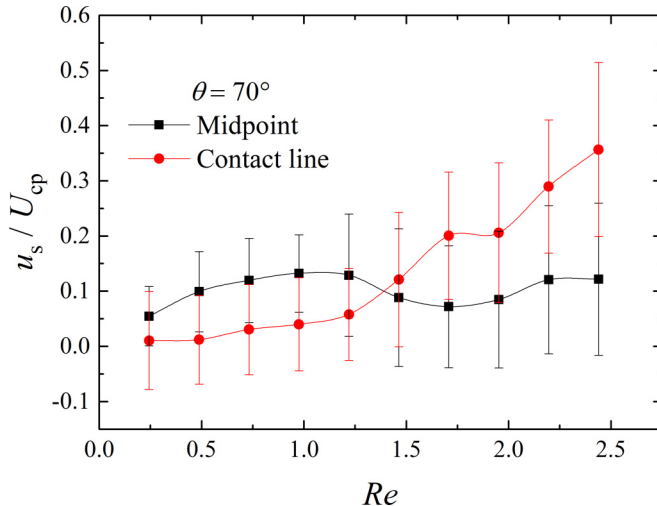
FIG. 13. The average velocity of slipping and thinning varying with Re on the surface of $\theta = 70°$.

pinch-off behaviors of liquid bridges according to discussion in the literature [31]. The variation of the minimal radius R_{min} of the thread versus breakup time is shown in Fig. 5. At the beginning the pinch-off process is affected by surface tension and inertial force with $R_{min} \sim (t_0 - t)^{2/3}$, where t_0 is the breakup time of the liquid bridge. Following with the decreasing of the thread radius, the effect of viscosity is increasingly important and the flow transits to an inertial-viscous regime. The relation between R_{min} and rupture time is linear in this region. Finally, the exponent becomes 0.418 when the pinch-off process is dominated by the thermal fluctuations [43]. The logarithmic plot in Fig. 5 shows that MDPD simulation can span three regions of pinch-off process, which was also observed by Arienti [31].

In summary, the simulated static profiles of liquid bridges between two plates and the dynamic spontaneous pinch-off process of a liquid cylinder are validated by theoretical predictions. It shows that the present MDPD model is feasible for studying the breakup behaviors of stretching liquid bridges.

III. RESULTS AND DISCUSSION

A. Symmetric surface wettability and stretching velocity

The stretching process with symmetric surface wettability and stretching velocity between two plates is simulated. All the lengths are normalized by the initial radius R_0 of the liquid bridge, and the Reynolds number $Re(= \rho U R_0 / \mu)$ is changed by imposing different plate stretching velocities.

Figure 6 shows the relationship between the minimum radius of the thread and the liquid bridge length H, in which the wettability on the upper and lower plates is the same, i.e., $\theta = 30°$, and three values of Re of 0.25, 1.46, and 2.5 are considered.

When stretching the liquid bridge, its middle part becomes thin and the liquid is squeezed away from the middle region with higher pressure resulting from surface tension, and the contact lines of the liquid bridge are pinned on the upper and lower plates. After the filament breaks at the middle of the liquid bridge, it decays into satellite drops, with the two main parts resting on the upper and lower plates, as shown in the snapshots of Fig. 6. This is consistent with previous experimental results [11,44]. Figure 6 also shows that for the given H the minimum radius increases with the increasing of Re.

Figure 7 shows the influences of surface wettability on the relation between the minimum radius of the liquid bridge and the bridge length H, in which Re is fixed at 0.25 and the contact angle θ is
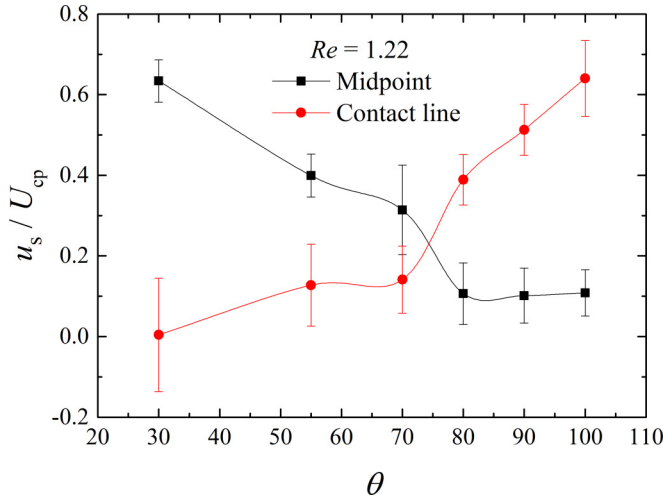
FIG. 14. The average velocities of slipping and thinning varying with θ for Re $= 1.22$.

changed from $30°$ to $70°$. It shows that the critical liquid bridge length H is affected by the surface wettability. For a given H, the minimum radius increases with the contact angle. For low Re, such as 0.25, surface tension alters the profiles of the liquid bridges from one equilibrium shape to another until breakup [6,7].

Furthermore, we increase Re to 1.22 for studying the influence of surface wettability on the position $Z_{r,min}$ of the minimum radius of the stretching liquid bridge. If the contact angle θ increases to $100°$, i.e., hydrophobic surfaces, the liquid bridge slips off the upper and lower plates, and the pinch-off occurs at both ends of the thread, forming a central droplet as shown in the snapshots of Fig. 8. $Z_{r,min}$ changes linearly with time for θ of $100°$, where the slope represents the plate stretching velocity.

The points distributing on the positive and negative sides of the Z axis for $\theta = 100°$ in Fig. 8 indicates that the position $Z_{r,min}$ of the minimum radius may occur at either the upper or lower
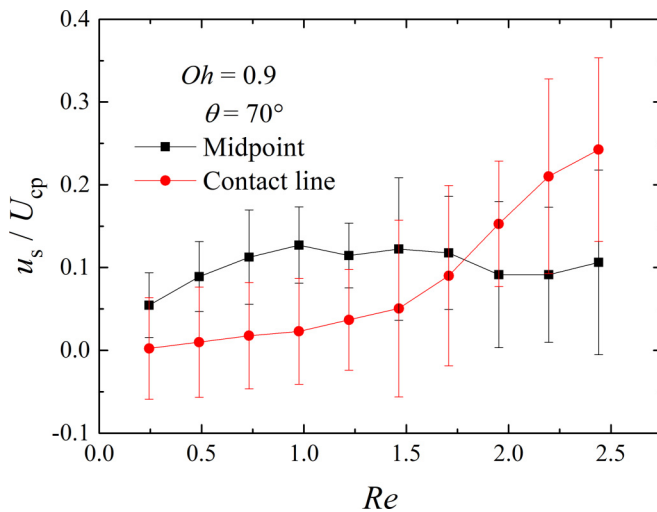

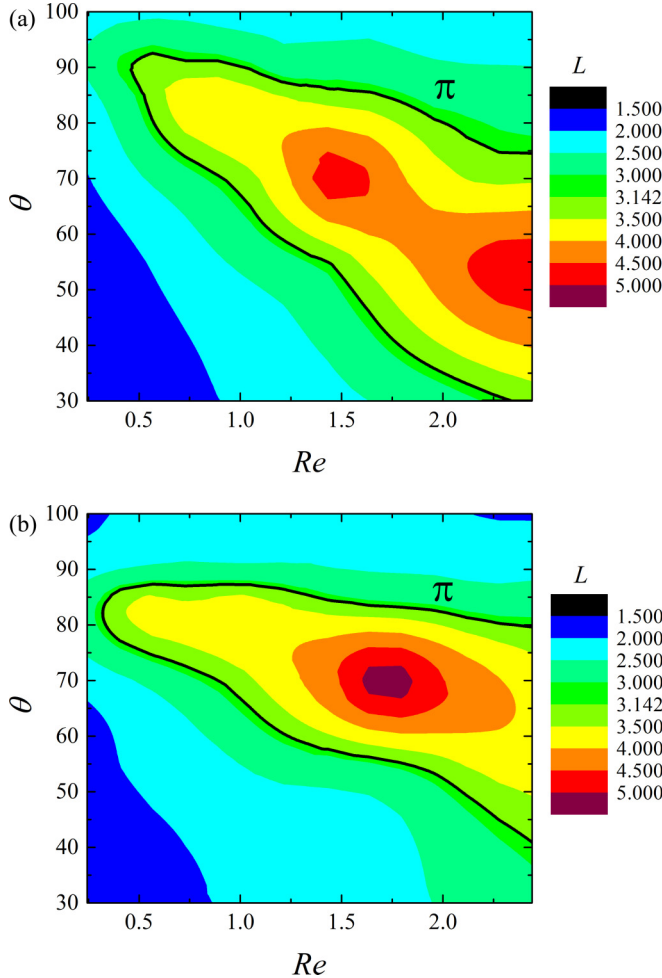FIG. 15. The average velocities of slipping and thinning varying with Re on the surface of $\theta = 70°$ for Oh $= 0.9$.

FIG. 16. The contour of the critical liquid bridge length L for different stretching velocities and surface wettability. (a) Oh = 0.3; (b) Oh = 0.9.

surface during stretching, while $Z_{r,min}$ fluctuates near zero for $\theta = 30°$, meaning that the position of the minimum radius is located near the middle of the thread for hydrophilic surfaces. It is interesting to note that $Z_{r,min}$ increases apparently when the liquid bridge approaches pinch-off, and $Z_{r,min}$ seems randomly to be at somewhere between the midpoint of the liquid bridge and the plate at the end. The detailed physical mechanism of this phenomenon is worthy of research in future work.

Figure 9 shows the variation of position Z_{break} of the pinch-off point with Re for different θ of 30°, 70°, and 100°. It shows that Z_{break} is unchanged regardless of Re on the surfaces of $\theta = 30°$ and 100°, in which Z_{break} is fixed approximately at zero for $\theta = 30°$ while it is equal to the diameter of the liquid bridge for $\theta = 100°$. In the two situations, the instability of the liquid bridge is affected by the competition between the slip velocity of the contact line and the thinning velocity of the liquid bridge, which are related to Re and surface wettability. The thinning velocity dominates the instability of the liquid bridge on hydrophilic surfaces; i.e., $\theta = 30°$ regardless of Re, and vice versa.

However, Z_{break} is dramatically affected by Re for $\theta = 70°$. In general, Z_{break} first rises slowly with increasing of Re; it jumps to the peak after Re is larger than approximately 1.22, and then falls off gradually. It shows that the pinch-off point shifts from the vicinity of the midpoint to the
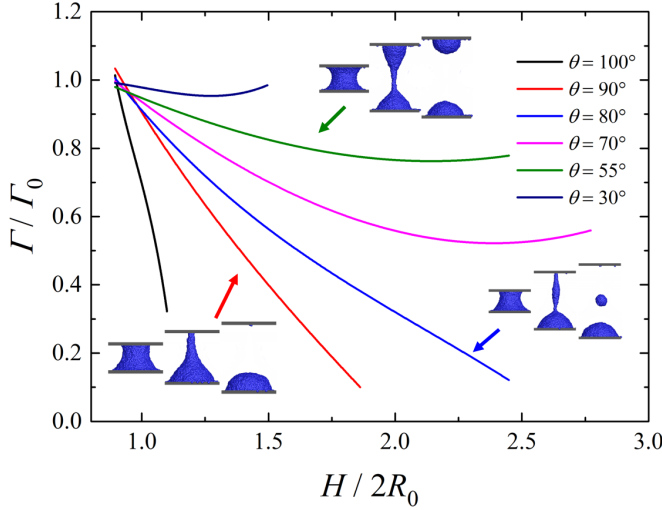
FIG. 17. The radius Γ of the contact line on the upper plate varying with the liquid bridge length.

plate, in which the dominant factor for liquid bridge instability depends on Re. In order to further display this shift, the variations of $Z_{r,min}$ during stretching are compared for Re = 1.22 and 1.46, as shown in Fig. 10. For Re = 1.22, the liquid bridge is stretched until it looks like a cylinder first, and then the liquid bridge thins with contact lines pinned. A long-lived filament is observed and it breaks somewhere other than midpoint. Filaments shrink quickly to merge with one of the two main droplets on both surfaces. This phenomenon is in agreement with previous experimental results [45,46]. The state of the liquid bridge is totally different if Re increases to 1.46, where the thread slips off both plates first; i.e., the pinch-off occurs around the contact lines first, forming a dumbbell shape. Then a filament emerges with itself decaying spontaneously into a satellite drop. Accordingly, $Z_{r,min}$ is located near zero at first and shifts to the position of the contact line at one moment, indicating that the key factor affecting the liquid bridge instability shifts from thinning of the liquid bridge to slipping of the contact line. The competition between the slip and thinning velocity is believed to be crucial for the breakup process and liquid transfer [9,11,47].

Figure 11 shows the variation of Γ with liquid bridge length, where θ is fixed at 70°, and Γ represents the radius of the contact line. Γ decreases first for all of Re, meaning that the contact lines on both plates retract at the beginning of stretching. However, for the smallest Re of 0.24, Γ quickly returns to its original value when the liquid bridge breaks. On the contrary, for other Re the radius Γ of the contact line decreases monotonously, and it reaches approximately zero finally for the largest Re of 2.44. It is worth noting the difference between the cases of Re = 1.22 and 1.46: For Re = 1.22 the contact line retracts first and is then pinned, but the contact line for Re = 1.46 continues to recede and accelerates until the liquid bridge slips off the plate.

The comparison between the slip velocity of the contact line and thinning velocity of the liquid bridge is shown in Fig. 12, where the error bar represents the value of the standard deviation of slip and thinning velocity. The speed and time are scaled by the capillary wave speed $U_{cp} = \sqrt{\sigma/\rho R_0}$ and time $t_{cp} = \sqrt{\rho R_0^3/\sigma}$. In Fig. 12(a), the slip and thinning velocity are approximately equal and both decrease with time until t/t_{cp} approaches 3.0, where u_s is the velocity of the slip of the contact line or the thinning of the liquid bridge. Then, the slip velocity continues to decline until the contact line is pinned on the plate, but the thinning velocity rises and it leads finally to the breakup near the midpoint of the liquid bridge. Figure 12(b) shows that when Re increases to 1.46 the slip velocity of the contact line rises in the later stage of the stretching and therefore results in the rupture of the liquid bridge near the surfaces. The competition between the slip and thinning velocity is related
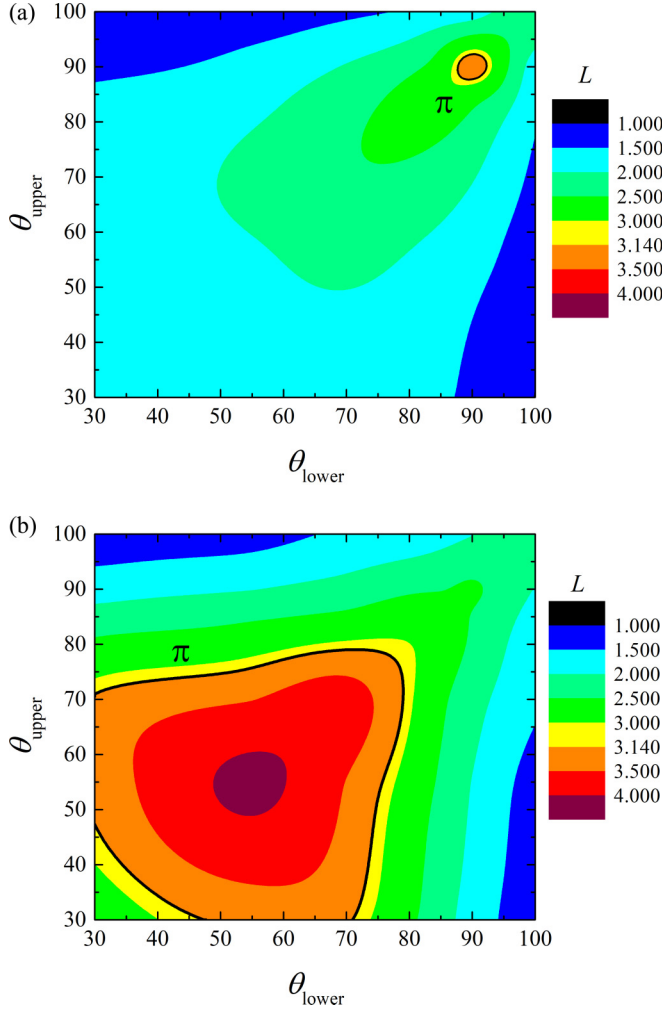
FIG. 18. The contour of the critical liquid bridge length on asymmetric wettability surfaces for different Re. (a) Re = 0.49; (b) Re = 1.95.

to the position of the liquid bridge breakup and it is directly affected by the stretching velocity as shown in Fig. 13.

Figure 13 shows the average velocity of slipping and thinning varying with Re on the surface of $\theta = 70°$. The slip velocity of the contact line increases with the increasing of Re. The slip velocity would exceed over the thinning velocity if Re is larger enough. The thinning velocity will decrease if slip velocity dominates the breakup process, since more liquids migrate from both ends to the middle.

The surface wettability is another factor influencing this competition [36,37]. Figure 14 shows the average velocities of slipping and thinning varying with θ for Re = 1.22. The contact line tends to slip quickly on hydrophobic surfaces, in contrast to the thinning velocity which gradually reduces with the increase of the contact angle.

Additionally, Oh is another key factor. Figure 15 shows the average velocities of slipping and thinning varying with Re on the surface of $\theta = 70°$ for Oh = 0.9, in which the features of the slip and thinning velocity are similar to those of Oh = 0.3 as shown in Fig. 13. However, the critical Re
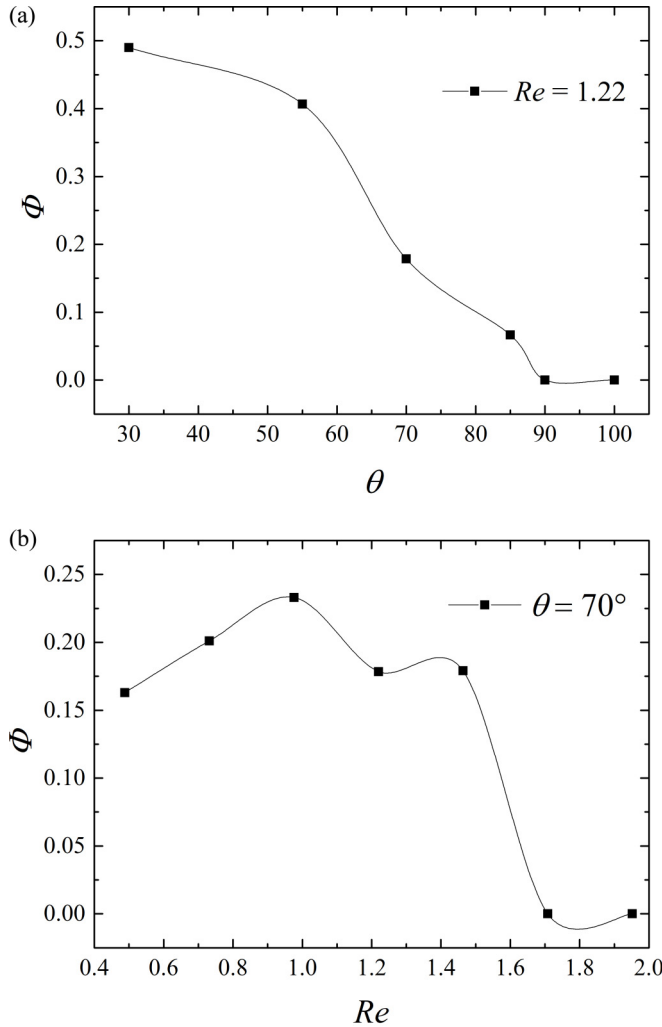
FIG. 19. (a) The liquid transfer Φ varying with different surface wettability on the upper plate for Re = 1.22. (b) Φ varying with Re for the contact angle on the upper plate, $\theta = 70°$.

for Oh = 0.9 is larger than that of Oh = 0.3, meaning that the viscous force enables the thread to be more stable [7].

Finally, the comprehensive influences of stretching velocity, surface wettability, and Oh on the critical liquid bridge length L are shown in Fig. 16, where the Rayleigh-Plateau limit is displayed as a reference. The Rayleigh-Plateau limit (RPL) states that the long cylinder becomes unstable when the wavelength exceeds its perimeter of the cross section, and RPL could be applicable when the quasistatic assumption of the surface tension is dominant [9]. In Fig. 16, RPL is the value of π due to the normalization of the liquid bridge length by $2R_0$, and it is represented by the black line in Fig. 16. The critical liquid bridge length is greater than RPL for large Re and small contact angle [8,9]. There are two peaks for the critical liquid bridge length of Oh = 0.3 compared with that of Oh = 0.9. Larger Oh provides stronger viscous effects to stabilize the liquid bridges, leading to a larger peak value of the critical liquid bridge length, i.e., 5.35 for Oh = 0.9, while it is 4.78 for Oh = 0.3. Actually the largest critical liquid bridge length is located at the region where the slip and thinning velocity are approximately equal to each other as shown in Fig. 15. The competition
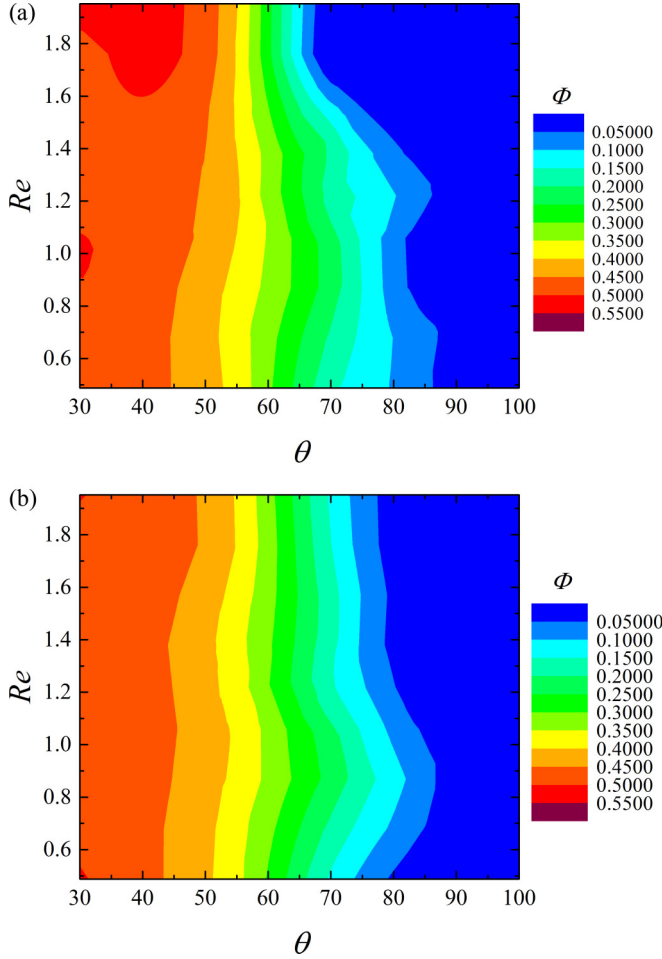
FIG. 20. The contour of Φ with different surface wettability and Re under asymmetric surface wettability. (a) Oh $= 0.3$; (b) Oh $= 0.9$.

between slip and thinning velocities is of great help to increase the critical liquid bridge length. This competition maybe the key factor for the dynamics of stretching liquid bridges and it is affected by stretching velocity, surface wettability, and Oh, respectively.

B. Asymmetric surface wettability

In lithographic printing, two chemically asymmetric plates are often adopted for the sake of controlling the liquid transfer ratio [4,5]. In this section the effects of asymmetric surface wettability on the competition between the slip of the contact line and the thinning of the liquid bridge are investigated.

Figure 17 shows the radius Γ of the contact line on the upper plate varying with the liquid bridge length H for Re $= 1.22$, in which the contact angle on the lower plate is fixed at $\theta = 30°$ with the wettability on the upper plate ranging from $30°$ to $100°$. The contact line slips quickly on the hydrophobic upper surfaces and results in a small critical liquid bridge length. The asymmetric surface wettability significantly affects the breakup dynamics of the stretching liquid bridges. As shown in Fig. 17, a filament is generated connecting with the main droplet for $\theta = 90°$, and the liquid bridge finally slips off the upper surface without leaving any remnant. The slip velocity of
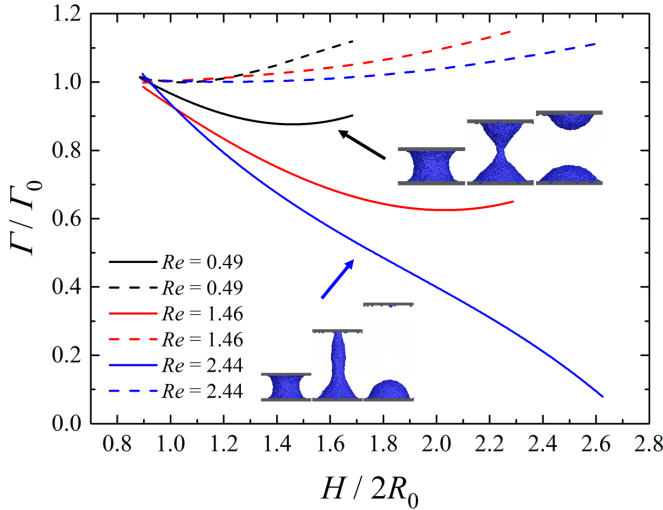
FIG. 21. The evolution of the position of the contact lines on the upper surface (solid lines) and on the lower surface (dashed lines) with different Re for $\theta = 55°$.

the contact line on the upper surface dominates the breakup process and leads to the liquid bridge pinching off near the upper surface. However, for a hydrophilic surface, i.e., $\theta = 55°$, the contact lines on both upper and lower plates recede slowly and the thinning velocity plays a conclusive role in rupture. It shows the liquid transfer ratio can be controlled by the surface wettability [5,9]. A large droplet is obtained on the lower plate for $\theta = 80°$; the small difference between slip and thinning velocity leads pinch-off occurring at both ends of the thread to form a large droplet on the lower plate, while leaving a small droplet in the middle which is undesirable in the printing process.

The influence of the asymmetric surface wettability on the critical liquid bridge length L is illustrated by Fig. 18, where the contact angles on the upper and lower plates are changed from $30°$ to $100°$, respectively. The region in which critical liquid bridge length exceeds RPL enlarges if increasing the Re from 0.49 to 1.95.

The aim of setting asymmetric surface wettability is to control the liquid transfer ratio between two plates. Hence, we concentrate on the liquid transfer ratio under the condition of asymmetric surface wettability. The liquid transfer ratio Φ is defined by the proportion of liquid mass on the top surface to the total mass of the liquid bridge. The contact angle on the lower surface is still fixed at $30°$. Figure 19(a) shows the effect of surface wettability on Φ, in which Φ decreases from 0.5 to 0 with the increase of the contact angle on the upper surface. Liquids tend to migrate from a nonwetting surface to a wetting surface. Figure 19(b) shows the variation of Φ with Re for constant wettability on the upper surface, i.e., $\theta = 70°$, while keeping the contact angle on the lower plate fixed at $30°$. For small Re, the thinning of the liquid bridge is dominant; Φ is relatively stable within the range of 0.15–0.25, regardless of plate stretching velocity. However, with the increase of Re, the slip velocity dominates the breakup process and Φ falls down to zero.

The influences of surface wettability on the upper plate, plate stretching velocity, and Oh on the liquid transfer ratio Φ are shown in Fig. 20, in which the contact angle on the lower plate is still kept at $30°$. Φ depends mainly on the asymmetry of surface wettability for small Re, as shown in Fig. 20(a). Larger wettability difference between upper and lower surface leads to small Φ. The liquid mass remaining on the top surface decreases due to increase of slip velocity for larger Re; namely, the blue region is broadened. However, this situation disappears for a liquid bridge with Oh = 0.9, as shown in Fig. 20(b). As we have discussed in the last section, higher viscous forces will reduce the slip velocity of the contact line and stabilize the liquid bridge, which increases Φ for high Re and the contact angle of about $70°$ on the upper plate.
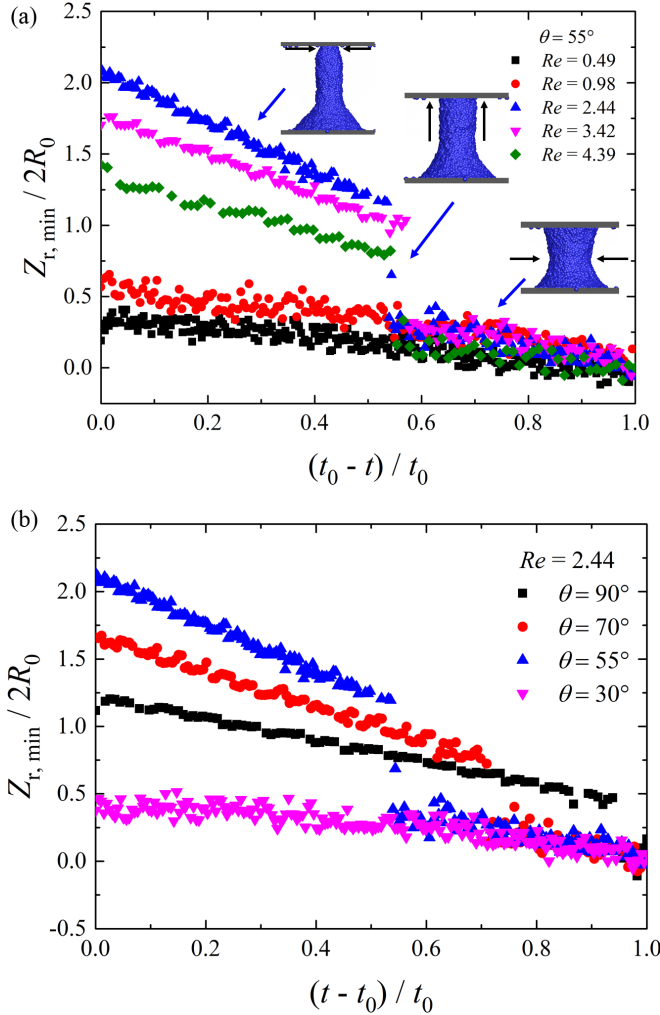
FIG. 22. The variation of the position of minimum radius versus breakup time. (a) The influences of Re for $\theta = 55°$; (b) the influences of surface wettability for Re = 2.44.

C. Asymmetric stretching velocity

In this section, the asymmetric stretching velocity is taken into consideration, which is common in the gravure printing process [5].

In this section, only the upper plate has imposed stretching velocity with a fixed lower plate. Additionally, the surface wettability on the two plates is identical. At first, we choose the surface of $\theta = 55°$. As shown in Fig. 21, the contact line on the lower surface is pinned, represented by dashed lines. Γ on the fixed lower surfaces gradually increases due to the migration of liquids from upper surfaces to the lower one. For small stretching velocity, i.e., Re = 0.49, the contact line on the top surface merely recedes a little and it is still pinned on the plate. Hence, two droplets rest on both plates, but their mass is not equal. For Re of 2.44 the position of the contact line declines monotonously until pinch-off occurs near the upper surface, meaning that Φ reaches zero.

Next, we focus on the variation of the position of minimum radius $Z_{r,min}$. Figure 22(a) shows that $Z_{r,min}$ increases slowly with stretching proceeding. Re has a minor effect on $Z_{r,min}$ at the beginning. This tendency will sustain if Re is small enough to prevent the liquid bridge from slipping off
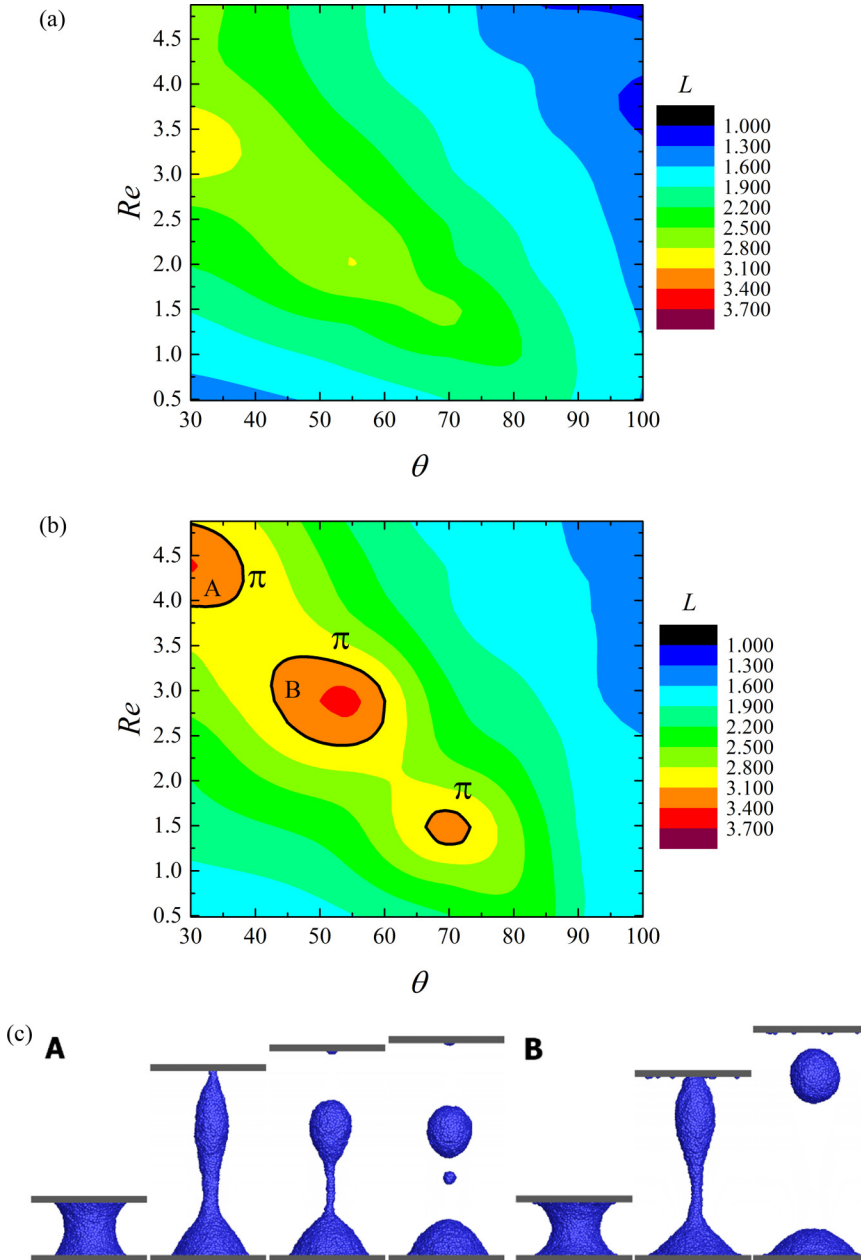
FIG. 23. The contours of the critical liquid bridge length for asymmetric stretching velocities. (a) Oh = 0.3; (b) Oh = 0.9. (c) The snapshots of stretching liquid bridges in regions A and B.

the upper plate. Nevertheless, the slip velocity surpasses the thinning velocity when Re increases, resulting in the faster reduction of Γ. At one moment Γ on the upper plate is equal to the value of the minimum radius, forming a cylindrical liquid bridge, as shown in the snapshot in Fig. 22(a). This status is vulnerable and changes immediately following with stretching. $Z_{r,min}$ jumps to the position of the upper surface and continues to increase due to the stretching of the upper plate. The moment of this jump seems to be independent of the stretching velocity and occurs half way through the
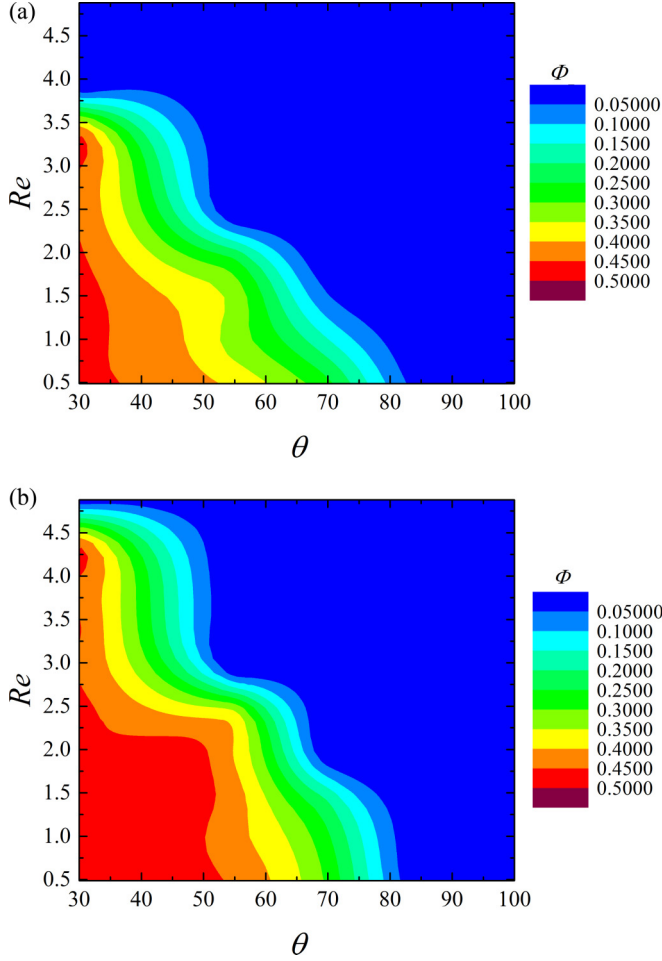
FIG. 24. The contour of Φ for different surface wettability and Re with asymmetric stretching velocities. (a) Oh = 0.3; (b) Oh = 0.9.

whole rupture process. Figure 22(b) shows that the moment of the jump is affected by the surface wettability. Stronger wettability delays the jump of minimum radius, meaning that the jump appears earlier on hydrophobic surfaces and then the motion of the contact lines dominates the breakup process.

Finally, the effects of Oh on the critical liquid bridge length and Φ are investigated as shown in Figs. 23 and 24, respectively. Compared with Figs. 23(a) and 23(b), it is found that the relations among surface wettability, Re, and critical liquid bridge length are similar qualitatively for different Oh. However, the region which is larger than RPL does not appear for small Oh (i.e., 0.3) under the asymmetric stretching velocity. On the contrary, there are three regions (i.e., regions A, B, and C) exceeding RPL for large Oh (i.e., 0.9).

Figure 23(c) shows the snapshots of stretching liquid bridges in regions A and B, respectively. The main difference between the two regions is the formation of satellite drops. A large droplet between the two plates and the residual on the lower plate are the main feature of regions A and B. However, the sequential order of appearance of the liquid bridge slipping off the surface and the breakup of the filament play a crucial role in the formation of satellite drops. In region A, the liquid bridge slips off the upper surface at first, and the thread connects the central droplet with the

residual part on the lower plate. This thread is then pinched off quickly and decays into satellite drops. On the contrary, in region *B* the thread breaks up before the slipping off of the liquid bridge; the ruptured thread retracts into droplets rapidly without generating satellite drops. According to this situation, we think that the competition between slip and thinning velocity is not only the key factor for the liquid transfer, but also for the formation of satellite drops. Like critical liquid bridge length, the distribution of Φ is qualitatively similar for different Oh (i.e., 0.3 and 0.9). If a liquid bridge needs to be divided into two identical parts, strong surface wettability and small stretching velocity are required. The complete liquid transfer from one surface to another would take place with increase of stretching velocity and poor surface wettability.

IV. CONCLUSION

A study on stretching liquid bridges between two flat plates was carried out by using many-body dissipative particle dynamics. At first, the simulated profile of the liquid bridge was validated. The agreement between the analytical solution and numerical results shows that reasonable effects of surface wettability can be captured in the simulation, and the spontaneous breakup process of the liquid bridge demonstrates that MDPD can span three regions of pinch-off process.

Next, for symmetric surface wettability and stretching velocity, it can be divided into three different rupture processes in terms of the position of the pinch-off point, which is affected by the surface wettability and stretching velocity. This difference is attributed to the competition between the slip of the contact line and the thinning of the liquid bridge. For strong surface wettability and small plate stretching velocity, thinning velocity dominates the breakup of the liquid bridge and the contact line is pinned on the plates. In contrast, the liquid bridge quickly slips off the plates for poor surface wettability and large plate stretching velocity, forming a droplet in the central region without remnants left on the plates. If the difference between slip and thinning velocity is small, the critical liquid bridge length apparently increases. This competition is influenced by surface wettability, plate stretching velocity, and Oh number.

The asymmetry of the contact angle reduces the critical liquid bridge length. The liquid mass transfer ratio Φ between two plates remains stable if the contact lines are pinned on the surfaces. Φ only depends on the asymmetry of surface wettability. However, Φ reaches zero with large stretching velocity due to the large slip velocity. For the asymmetric stretching velocity, the sudden jump of the position of minimum radius is analyzed with different stretching velocities and surface wettabilities. The moment of the jump is determined by surface wettability rather than stretching velocity. Moreover, the formation of satellite drops is related to the sequential order of appearance of the liquid bridge slipping off the plate and the breakup of the filament.

In summary, it demonstrates that the competition between slip and thinning velocity determines the breakup dynamics of the stretching liquid bridges, resulting in different liquid transfer ratio. This competition can be managed by adjusting surface wettability, plate stretching velocity, and liquid property such as Oh number, respectively. This work may provide some insights into ink printing technology where the accuracy of liquid transfer is required.

---

[1] J. Plateau, *Experimental and Theoretical Statics of Liquids Subject to Molecular Forces Only* (Gauthier-Villars, Paris, 1873).

[2] L. Rayleigh, On the instability of jets, Proc. London Math. Soc. **10**, 4 (1878).

[3] L. Rayleigh, On the capillary phenomena of jets, Proc. London Math. Soc. **29**, 71 (1879).

[4] O. A. Basaran, H. Gao, and P. P. Bhat, Nonstandard inkjets, Annu. Rev. Fluid Mech. **45**, 85 (2013).

[5] S. Kumar, Liquid transfer in printing processes: Liquid bridges with moving contact lines, Annu. Rev. Fluid Mech. **47**, 67 (2015).

[6] R. Kröger, S. Berg, A. Delgado, and H. J. Rath, Stretching behaviour of large polymeric and Newtonian liquid bridges in plateau simulation, J. Non-Newtonian Fluid Mech. **45**, 385 (1992).

[7] X. Zhang, R. S. Padgett, and O. A. Basaran, Nonlinear deformation and breakup of stretching liquid bridges, J. Fluid Mech. **329**, 207 (2006).

[8] C. Gupta, G. A. Mensing, M. A. Shannon, and P. J. A. Kenis, Double transfer printing of small volumes of liquids, Langmuir **23**, 2906 (2007).

[9] S. Dodds, M. Carvalho, and S. Kumar, Stretching and slipping of liquid bridges near plates and cavities, Phys. Fluids **21**, 092103 (2009).

[10] S. Dodds, M. Carvalho, and S. Kumar, Stretching liquid bridges with moving contact lines: The role of inertia, Phys. Fluids **23**, 092101 (2011).

[11] B. Qian and K. S. Breuer, The motion, stability and breakup of a stretching liquid bridge with a receding contact line, J. Fluid Mech. **666**, 554 (2011).

[12] J. Eggers, Nonlinear dynamics and breakup of free-surface flows, Rev. Mod. Phys. **69**, 865 (1997).

[13] S. Kawano, Molecular dynamics of rupture phenomena in a liquid thread, Phys. Rev. E **58**, 4468 (1998).

[14] Y. S. Choi, S. J. Kim, and M. U. Kim, Molecular dynamics of unstable motions and capillary instability in liquid nanojets, Phys. Rev. E **73**, 016309 (2006).

[15] H. Shin, D. Suh, and W. Yoon, Non-equilibrium molecular dynamics of nanojet injection in a high pressure environment, Microfluid. Nanofluid. **5**, 561 (2008).

[16] P. Zhu, X. Tang, Y. Tian, and L. Wang, Pinch-off of microfluidic droplets with oscillatory velocity of inner phase flow, Sci. Rep. **6**, 31436 (2016).

[17] A. U. Chen, P. K. Notz, and O. A. Basaran, Computational and Experimental Analysis of Pinch-Off and Scaling, Phys. Rev. Lett. **88**, 174501 (2002).

[18] Moseler and U. Landman, Formation, stability, and breakup of nanojets, Science **289**, 1165 (2000).

[19] J. Lin, Studying on water nanojet ejection and the wetting phenomena on the nozzle surface, Microfluid Nanofluid. **13**, 37 (2012).

[20] H. Shin, M. Oschwald, M. M. Micci, and W. Yoon, Influence of thermodynamic state on nanojet break-up, Nanotechnology **16**, 2838 (2005).

[21] A. Tiwari, H. Reddy, S. Mukhopadhyay, and J. Abraham, Simulations of liquid nanocylinder breakup with dissipative particle dynamics, Phys. Rev. E **78**, 016305 (2008).

[22] R. F. Fox and G. Uhlenbeck, Contributions to non-equilibrium thermodynamics. I. Theory of hydrodynamical fluctuations, Phys. Fluids **13**, 1893 (1970).

[23] P. J. Hoogerbrugge and J. M. V. A. Koelman, Simulating microscopic hydrodynamic phenomena with dissipative particle dynamics, Europhys. Lett. **19**, 155 (1992).

[24] P. Español, Hydrodynamics from dissipative particle dynamics, Phys. Rev. E **52**, 1734 (1995).

[25] R. D. Groot and P. B. Warren, Dissipative particle dynamics: Bridging the gap between atomistic and mesoscopic simulation, J. Chem. Phys. **107**, 4423 (1997).

[26] P. Español and P. B. Warren, Statistical mechanics of dissipative particle dynamics, Europhys. Lett. **30**, 191 (1995).

[27] C. J. Mo, L. J. Yang, F. Zhao, and K. D. Cui, Mesoscopic simulation of a thinning liquid bridge using the dissipative particle dynamics method, Phys. Rev. E **92**, 023008 (2015).

[28] A. Tiwari and J. Abraham, Dissipative particle dynamics simulations of liquid nanojet breakup, Microfluid Nanofluid. **4**, 227 (2008).

[29] J. R. Lister and H. A. Stone, Capillary breakup of a viscous thread surrounded by another viscous fluid, Phys. Fluids **10**, 2758 (1998).

[30] P. B. Warren, Vapour-liquid coexistence in many-body dissipative particle dynamics, Phys. Rev. E **68**, 066702 (2003).

[31] M. Arienti, W. Pan, X. Li, and G. E. Karniadakis, Many-body dissipative particle dynamics simulation of liquid/vapor and liquid/solid interactions, J. Chem. Phys. **134**, 204114 (2011).

[32] J. Y. Zhao and S. Chen, Following or against topographic wettability gradient: movements of droplets on micropatterned surface, Langmuir **33**, 5328 (2017).

[33] J. Y. Zhao, S. Chen, and Y. Liu, Spontaneous wetting transition of droplet coalescence on immersed micropillared surfaces, Appl. Math Modell. **63**, 390 (2018).

[34] K. X. Zhang, Z. Li, M. Maxey, S. Chen, and G. E. Karniadakis, Self-cleaning of hydrophobic rough surfaces by coalescence-induced wetting transition, Langmuir **35**, 2431 (2019).

[35] J. Y. Zhao, S. Chen, and N. Phan-Thien, Viscometric flow for a many-body dissipative particle dynamics (MDPD) fluid with Lees-Edwards boundary condition, Mol. Simul. **44**, 213 (2018).

[36] C. Cupelli, B. Henrich, T. Glatzel, R. Zengerle, M. Moseler, and M. Santer, Dynamic capillary wetting studied with dissipative particle dynamics, New J. Phys. **10**, 043009 (2008).

[37] C. Chen, C. Gao, L. Zhuang, X. Li, P. Wu, J. Dong, and J. Lu, A many-body dissipative particle dynamics study of spontaneous capillary imbibition and drainage, Langmuir **26**, 9533 (2010).

[38] Y. Wang, S. Chen, and Y. Liu, Spontaneous uptake of droplets into non-wetting capillaries, Comput. Fluids **136**, 1 (2016).

[39] C. Delaunay, Sur la surface de revolution dont la courbure moyenne est constante, J. Math. Pures Appl. **6**, 309 (1841).

[40] E. J. De Souza, M. Brinkmann, C. Mohrdieck, A. Crosby, and E. Arzt, Capillary forces between chemically different substrates, Langmuir **24**, 10161 (2008).

[41] H. Kusumaatmaja and R. Lipowsky, Equilibrium morphologies and effective spring constants of capillary bridges, Langmuir **26**, 18734 (2010).

[42] Y. X. Wang, S. Michielsen, and H. J. Lee, Symmetric and asymmetric capillary bridges between a rough surface and a parallel surface, Langmuir **29**, 11028 (2013).

[43] J. Eggers, Dynamics of Liquid Nanojets, Phys. Rev. Lett. **89**, 084502 (2002).

[44] J. Meseguer, Stability of slender, axisymmetric liquid bridges between unequal disks, J. Cryst. Growth **67**, 141 (1984).

[45] C. Wagner, Y. Amarouchene, D. Bonn, and J. Eggers, Droplet Detachment and Satellite Bead Formation in Viscoelastic Fluids, Phys. Rev. Lett. **95**, 164504 (2005).

[46] T. R. Tuladhar and M. R. Mackley, Filament stretching rheometry and break-up behavior of low viscosity polymer solutions and inkjet fluids, J. Non-Newtonian Fluid Mech. **148**, 97 (2008).

[47] W. Villanueva, J. Sjödahl, M. Stjernström, J. Roeraade, and G. Amberg, Microdroplet deposition under a liquid medium, Langmuir **23**, 1171 (2007).